J Sol-Gel Sci Technol (2016) 77:205–210
DOI 10.1007/s10971-015-3845-7

ORIGINAL PAPER

Two novel sol–gel-derived nanostructures and their hemoglobin sensing features

Zhan Zhou[2] · Yuhui Zheng[2] · Jinwei Gao[4] · Lasheng Jiang[2] · Qianming Wang[1,2,3]

Received: 27 June 2015 / Accepted: 14 August 2015 / Published online: 2 September 2015

Abstract Sol–gel-derived nanosilica materials covalently anchored by functionalized terbium complexes with different dimensions were prepared. Zero-dimensional hybrid had a diameter of 50 nm with regular spherical shape. The lengths and widths of 1D nanorod hybrid were in the range of 50–70 and 20–30 nm. The specific surface areas of the two-dimensional materials were 81 and 108 cm^2/g, respectively. Both materials bind hemoglobin in aqueous buffer solution (pH 7.4) as shown by striking luminescence changes. These novel findings will pave the way for the application of novel nanostructured lanthanide hybrids in sensor devices.

Graphical Abstract

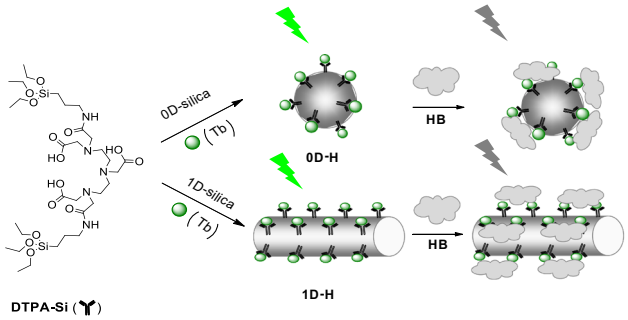

Keywords Terbium · Luminescence · Quenching · Hemoglobin

1 Introduction

Heme-containing protein such as hemoglobin (HB) is widely distributed in erythrocyte which has been closely related to binding oxygen, electron transfer and catalysis in biological pathways [1, 2]. Chemical sensing using fluorescence to monitor an analyte has been fully developed based on a wide variety of organic chromophores. But their short-lived emissions with broad bands were frequently affected by the other noise signals in most biological systems. Lanthanide complexes have very long radiative lifetimes with narrow-line emissions, and time-gated detection method could be used [3, 4]. Currently, the detection of free hemoglobin could be realized through the design of functional terbium complexes, and the utilization of the metal-centered luminescence exhibited promising potentials in the fields of bio-analysis [5–8]. But the pure

Electronic supplementary material The online version of this article (doi:10.1007/s10971-015-3845-7) contains supplementary material, which is available to authorized users.

✉ Yuhui Zheng
yhzheng78@scnu.edu.cn

✉ Qianming Wang
qmwang@scnu.edu.cn

[1] Key Laboratory of Theoretical Chemistry of Environment, Ministry of Education, School of Chemistry and Environment, South China Normal University, Guangzhou 510006, People's Republic of China

[2] School of Chemistry and Environment, South China Normal University, Guangzhou 510006, People's Republic of China

[3] Guangzhou Key Laboratory of Materials for Energy Conversion and Storage, Guangzhou 510006, People's Republic of China

[4] Institute for Advanced Materials, Academy of Advanced Optoelectronics, South China Normal University, Guangzhou 510006, People's Republic of China

emissive lanthanide complexes would be sensitive to vibrational quenching by energy migration to adjacent coordinated water molecules or polar solvents. In addition, the metal complexes lack enough thermal stability, mechanical strength, rigidity and photostability. Therefore, the emergence of functional hybrid materials could meet the requirement for future uses and lie between the interface of the organic and inorganic realms, which had high versatility for assembling tailor-made materials. In this field, sol–gel treatment with low-processing temperature and easy steps permits the fabrication of two phases within nanometer scale [9]. Furthermore, the performance of using lanthanide emission signals in the sol–gel-derived matrix to study the host–guest interactions has received considerable attention [10–12]. However, the classical physical doping techniques would result in concentration-based quenching, particle aggregation or phase separation due to the weak interactions [13, 14]. Hybrid inorganic–organic materials with strong covalent bonds linked the interface circumvent these drawbacks. Previous literatures have discussed these types of covalent linkages in the sensing materials, and generally, the ligand used only had a single triethoxy silane group to bind with inorganic host [15, 16]. In view of the structure design, we have developed a novel double-armed silylated ligand (triethoxysilylpropyl)diethylenetriaminetetraacetic acid) with polydentate coordinate sites to firmly combine terbium complex and inorganic backbone. The strong grafting force between the organic and inorganic moieties would certainly improve its stability and efficiency. Additionally, we assembled zero-dimensional lanthanide-based hybrid nanospheres with very uniform diameters ($\sim$50 nm) (abbreviated as 0D-H) and also the regular one-dimensional nanostructures (Fig. S1). To our knowledge, it has been regarded as the first example of the controllable syntheses and comparison of terbium complex-appended-dimensional nanoarchitectures for the detection of specific target. The resultant intensive green emission was selectively responsive to hemoglobin (HB) but not human serum albumin (HSA), lysozyme (LZ) or trypsin (TP).

2 Materials and methods

Terbium perchlorate was obtained by dissolving Tb_4O_7 in concentrated perchloric acid. Human serum albumin, hemoglobin, trypsin and lysozyme were purchased from Aldrich. Polyoxyethylene (20) cetyl ether (Brij 58), aminopropyltriethoxysilane (APS, 99 %), diethylenetriamine pentaacetic acid dianhydride (DTPAda, 98 %), hydrazine-hydrate (100 %, hydrazine 80 %) and tetraethyl orthosilicate (TEOS) were purchased from J&K Scientific. ^{1}H-NMR spectra were recorded at 293 K using a Varian 400 (400 MHz) with TMS as an internal standard. Fluorescence spectra and quantum yields were measured using an Edinburgh FLS920 spectrometer (Great Britain). FTIR spectra were measured using a Shimadzu Prestige-21. TEM was measured using a JEOL JEM-2100HR transmission electron microscope. SEM analysis data were measured using a Zeiss Ultra 55 scanning electron microscope. The adsorption desorption isotherms of nitrogen were measured at 77 K using the ASAP2020M system. The morphological control of nanoscale materials was performed based on literatures [17, 18].

2.1 Synthesis of precursor DTPA-Si

DTPAda (1 g, 2.8 mmol) was dissolved in 55 mL of anhydrous pyridine under a steady flow of nitrogen, and aminopropyltriethoxysilane (1.37 g, 6.2 mmol) was added with magnetic stirring. The mixture was stirred under nitrogen for 24 h at room temperature. The product was then precipitated with the addition of hexane to remove excess aminopropyltriethoxysilane, isolated by centrifuging, washed with additional aliquots of hexanes and dried in a vacuum to obtain the target compound (DTPA-Si). MS (LCMS): *m/z* 798.9 $[M–H]^-$. NMR: ^{1}H (DMSO, ppm): 0.53 (t, 4H), 1.16 (t, 18H), 1.43(p, 4H), 2.83 (t, 4H), 2.91 (t, 4H), 3.05 (q, 4H), 3.21 (s, 6H), 3.36 (s, 4H), 3.69 (q, 12H), 8.11 (t, 2H).

2.1.1 Synthesis of Tb–DTPA-Si complex

DTPA-Si (0.52 g, 0.65 mmol), $Tb(ClO_4)_3$ (13 mL of a 0.05 M solution, 0.65 mmol) and ammonia (1 mL) were added together. The mixture was stirred for 5 h at room temperature. The crude product was washed with ethanol and water and then dried in vacuo overnight. The resulting precipitate was collected to give the desired Tb–DTPA-Si as white powder.

2.2 Fabrication of 0D silica nanoparticles

The fabrication of 0D silica nanoparticles was performed based on the previous Ref. [17]. In a 250-mL glass flask, 17.7 g of Triton X-100, 16 mL of n-hexanol and 75 mL of cyclohexane were mixed with forceful magnetic stirring, and 4 mL deionized H_2O was added. After addition of 1 mL TEOS, the solution was stirred for 30 min; 0.65 mL of NH_4OH was added. This polymerization was allowed to proceed for 18 h. The particles were centrifuged, sonicated and vortexed three times with anhydrous ethanol, followed by washing twice with deionized water and dried under vacuum to obtain the silica nanoparticles.

2.3 Fabrication of the terbium complex-loaded-zero-dimensional hybrid material (0D-H)

In the silica nanoparticle (0.3 g) suspension, 1 mL DTPA-Si DMSO solution (0.5 M) and 0.5 mL of aqueous ammonia were added, and the suspension was stirred for 5 h. $Tb(ClO_4)_3$ solution (1 mL, 0.5 M) was added. After 12 h, the precipitate was centrifuged and redispersed in water at least three times to remove excess unreacted DTPA-Si and terbium ions and dried under vacuum to give the hybrid material (0D-H). We have to mention that the spherical nanoparticles described by the literature were used as the efficient solid matrix to load the terbium complex, and the stability has been enhanced. We focused more on the photophysical features and sensing behavior by using lanthanide line emissions.

2.4 Fabrication of 1D silica nanorods

Currently, a few references have concentrated on the synthesis of low-dimensional nanocrystals through directional growth method, and various templates such as polymers and silver nanowires were used [19–21]. Here we try to adopt the nickel–hydrazine complex as the controllable template to afford the one-dimensional nanostructures according to the previous Ref. [18]. The detailed synthesis was described as follows: 8.5 g of Brij 58 was dissolved in 15 mL of cyclohexane and was kept at 50 °C. Then, 1.9 mL of 0.8 M $NiCl_2$ was added, and 0.45 mL of hydrazine hydrate was added dropwise. After 3 h stirring, 1 mL of diethylamine and 3 mL of TEOS were added. The silica coating process was allowed to proceed for 2 h. The precipitates were dispersed in 300 mL of 1 M HCl and stirred at room temperature for 1 h. The silica nanorods (1D) were retrieved by centrifugation and washed with water until neutral pH was reached.

2.5 Fabrication of 1D nanorod hybrid material (1D-H)

In the silica host (1D nanorod, 0.3 g) suspension, 1 mL DTPA-Si DMSO solution (0.5 M) and 0.5 mL of aqueous ammonia were added, and the suspension was stirred for 6 h. $Tb(ClO_4)_3$ solution (1 mL, 0.5 M) was added. After 10 h, the precipitate was centrifuged and redispersed in water at least three times to remove excess unreacted DTPA-Si and terbium ions. Then, the 1D nanorod hybrid material (1D-H) was obtained after drying under vacuum for overnight.

3 Results and discussion

Formation of an amide linkage between DTPAda and the primary amine group of aminopropyl triethoxysilane was confirmed by bands located at 788 cm^{-1} (N–H bending mode), 1086 cm^{-1} (Si–O) 1631 cm^{-1} (amide I) and 2970 and 2921 cm^{-1} (the asymmetric and symmetric stretching vibrations of CH_2 groups of the alkyl chains) (Fig. S2a). In the curve for sample 0D-H (Fig. S2b), the "amide I" absorption band shifted from 1631 to 1598 cm^{-1}, indicating coordination between the carboxylate and the terbium ion [22]. Similar results were observed in FTIR spectra of 1D-H (Fig. S2c).

Transmission electron microscopy (TEM) was used to determine the size and morphology of 0D-H and 1D-H (Fig. 1). 0D-H exhibited a monodispersed spherical morphology with a diameter of approximately 50 nm, and no observable change was seen in morphology after the organic chromophores were covalently coated onto the silica host (Fig. 1a). 1D nanorods were obtained in large quantities as illustrated in Fig. 1b. The lengths and widths were in the range of 50–70 and 20–30 nm, respectively. This novel luminescent terbium-sensitized 1D nanostructure will be ideal for use in dimensionally confined functional devices.

The photoluminescence spectra of 0D-H and 1D-H in buffer (5 mM Tris–HCl, 50 mM NaCl, pH 7.4) in the absence of HB were given in Fig. S3. The corresponding curves were collected at room temperature and the emission range covered from 450 to 650 nm. The excitation wavelength has been set as 272 nm. The absorbed energy was contributed by ligands and migrated to the terbium ions through the antenna effect [4]. The sharp and narrow emission peaks correspond to transitions between the excited $5D_4$ level and various J-levels of the ground state ^7F_J ($J = 6, 5, 4$, and 3). It was noticed that the most intense peak in the visible region is the $^5D_4 \rightarrow {}^7F_5$ transition, and it was well located in the green area. The quantum yields measured using an integrating sphere was 8.9 % (1D-H) and 7.7 % (0D-H), respectively. Moreover, we have investigated the photostability behavior of 1D-H and its complex (Tb–DTPA-Si complex). 1D-H presented much enhanced photostability in contrast to Tb–DTPA-Si complex (Fig. S4). Both materials were exposed under the irradiation by an electric incandescent lamp (60 W). Tb–DTPA-Si complex has demonstrated 50 % reduction in peak intensity, whereas 1D-H has maintained to be almost stable in its original emission (less than 9 %).

Upon addition of HB in the concentration range from 0.2 to 30 μM, the intensity of emissions from 1D-H decreased linearly; emission was almost completely quenched at 30 μM HB (Fig. 2). The relative luminescence intensity decreased from 876 to 189 within 3–4 s of addition of HB, and the striking change could be observed by the naked eye under a 254-nm UV lamp. The quenching effect (F_0/F) versus the concentration (from 0.2 to 30 μM) of HB fit the simple linear equation $y = 0.9880 + 0.1085x$ ($R^2 = 0.999$). The detection limit for HB was

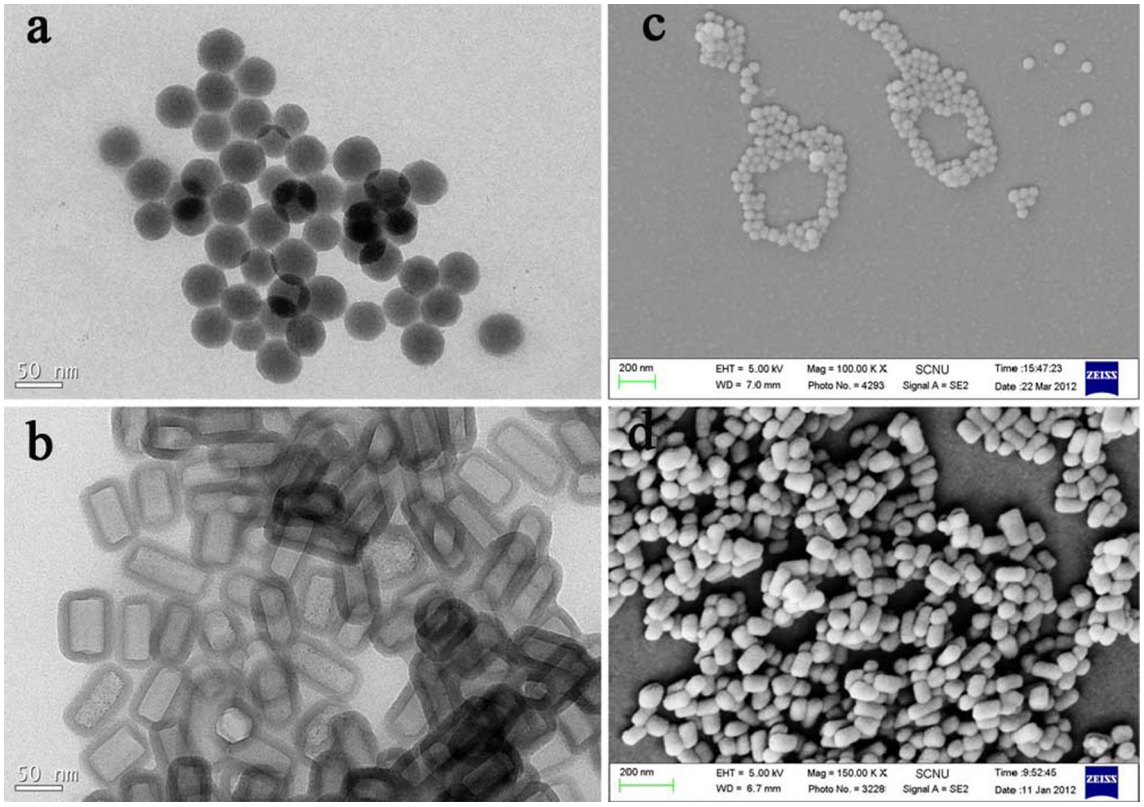

Fig. 1 TEM (*left*) and SEM (*right*) images of **a**, **c** 0D-H, **b**, **d** 1D-H

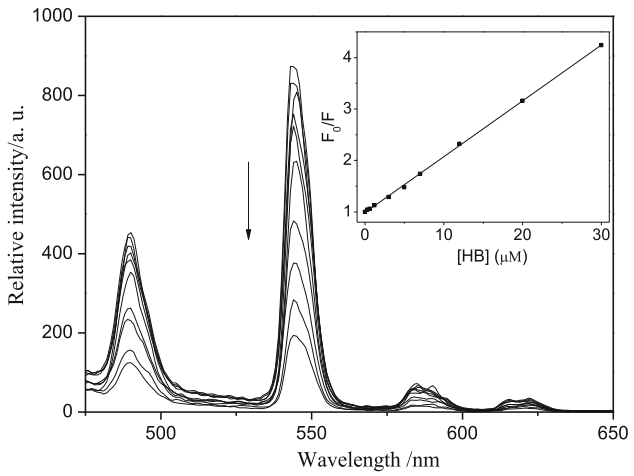

Fig. 2 Emission spectra of 1D-H (5 mg/L) upon addition of 0.2–30 μM HB in buffer (5 mM Tris–HCl, 50 mM NaCl, pH 7.4). *Inset* Plot of F_0/F versus the concentration of HB shows a linear relationship

calculated to be 1.2 μM by using the equation DL = 3 × SD/S with a signal-to-noise ratio of 3 (DL means detection limit; SD means the standard deviation; S refers to the slope of calibration curve) [23]. Parallel experiments were carried out ten times, and the relative standard deviation was calculated to be 4.34 %. In a similar fashion, the emission of 0D-H also decreased stepwise in the presence of increasing HB (from 0.2 to 30 μM, Figure S5). The calibration curve also follows a simple linear function [$y = 0.9925 + 0.0933x$ ($R^2 = 0.997$)]. The ability of 1D-H to detect HB was slightly better than 0D-H material (1.5 μM) (Fig. S5). These data prove that binding is dependent on morphological structure.

In order to confirm the selectivity of these sensors, other related proteins such as HSA, LZ or TP with much higher concentrations (150 μM) were added in the above solutions (Fig. 3). All the experiments were measured for three times, and the average peak emission intensities were used. As provided in Fig. 3, although HSA, LZ or TP could slightly decrease the luminescence (the reduction in intensities were within 10 %), the effects were much less than that of HB. Analogous experiments were performed with 0D-H, and similar phenomena were observed. The results showed that these nanoprobes have a high selectivity for HB and could be potentially applied as luminescent sensors for this protein in aqueous solution. It suggested that other proteins did not interact with the lanthanide organic–inorganic nanostructures and the selectivity would be closely related to the unique functional groups and molecular structures of HB.

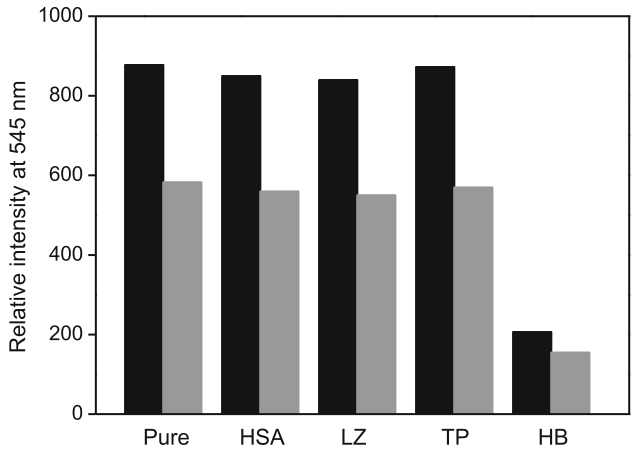

Fig. 3 Selectivity of 1D-H (*black*) and 0D-H (*gray*) for HB. The concentrations of the all proteins were 150 μM with the exception of HB which was 30 μM. All experiments were performed in 5 mM Tris–HCl, 50 mM NaCl (pH 7.4)

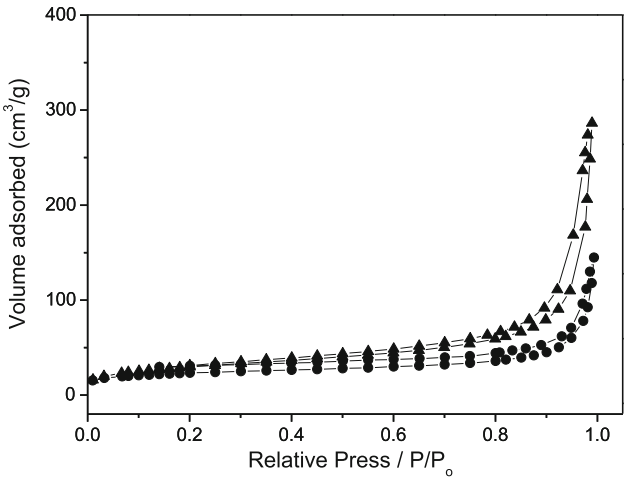

Fig. 4 Nitrogen adsorption–desorption curves of 1D-H (*filled triangle*) and 0D-H (*filled circle*)

The HB molecule possesses four globular protein subunits, and each subunit contains a protein chain linked with a nonprotein heme group that mainly consists of protoporphyrins. These macrocyclic ligands coordinate with lanthanide ions through pyrrolic nitrogen atoms, and functional metalloporphyrins (double-decker type) have been assembled [24]. Based on our sensors, we hypothesize that the heme moiety interacts with terbium ions to alter the original coordination structure between Tb^{3+} and DTPA-Si. Because the triplet state energy level of protoporphyrin is much lower (<16,000 cm^{-1}) than the excited state of terbium ions (20,400 cm^{-1}), insertion of terbium ion into protoporphyrin prevents the energy of the donor's triplet state from migrating to the acceptor (Tb^{3+}) [25]. Thus, in the presence of HB, the characteristic terbium emission of the nanostructures disappears. None of the other proteins tested have heme groups, so no changes in emission were observed in their presence.

The specific surface area (108 cm^2/g) of 1D-H was larger than 0D-H (81 cm^2/g) as shown by adsorption–desorption isotherms of nitrogen (Fig. 4). Particularly, the total pore volume of the former was determined to be 0.27 $cm^3\ g^{-1}$, and the value was higher than its counterparts (0D-H: 0.12 $cm^3\ g^{-1}$). This will allow more HB molecules to contact with the silica walls in the 1D-H nanostructure than in the other case. In addition, reusability experiments were performed by rinsing the collected powders with ethanol and water five times for each case. Notably, 1D-H displayed much better reusability than 0D-H and small reduction in the emissions was detected after ten repeated circles (Fig. S6). The collected results showed the hybrid composite with large aspect ratio might provide specific capacity to load enough lanthanide complexes due to its internal surface area and inherent nanostructures. Therefore, the green fluorescence from emissive terbium complex could be maintained after the recovery experiments.

4 Conclusions

In summary, two kinds of cross-linked siloxane hybrid terbium nanocomposites with different dimensional shapes were assembled. The photoluminescence properties, surface area, recognition behavior and reusability of the two hybrid inorganic–organic materials have been extensively discussed. The results show that the sol–gel-derived optical probes will be promising in the analytical field.

Acknowledgments Q. M. acknowledges the support from National Natural Science Foundation of China (No. 21371063), excellent university young scholar fund of Guangdong Province (Yq2013053), Guangzhou city scientific research fund (2014J4100054) and Guangdong Science and Technology plan (2013B010403025).

References

1. Pakapongpan S, Palangsuntikul R, Surareungchai W (2011) Electrochim Acta 56:6831–6836
2. del Valle-Mondragon L, Ramirez-Ortega M, Zarco-Olvera G, Sanchez-Mendoza A, Pastelin-Hernandez G, Tenorio-Lopez FA (2008) Talanta 74:478–488
3. Parker D (2000) Coord Chem Rev 205:109–130
4. Bunzli JCG, Piguet C (2005) Chem Soc Rev 34:1048–1077
5. Aime S, Fasano M, Paoletti S, Bellelli A, Coletta M, Ascenzi P (1998) J Inorg Biochem 71:37–43
6. Cheng Y, Lin HK, Xue DP, Li RC, Wang K (2001) Biochim Biophys Acta 1535:200–216
7. Morgner F, Lecointre A, Charbonniére LJ, Lohmannsroben HG (2015) Phys Chem Chem Phys 17:1740–1745
8. Yegorova AV, Leonenko II, Aleksandrova DI, Scrypynets YV, Antonovich VP, Ukrainets IV (2014) J Appl Spectrosc 81:672–677

9. Liu FY, Fu LS, Wang J, Meng QG, Li HR, Guo JF, Zhang HJ (2003) New J Chem 27:233–235
10. Motorina A, Tananaiko O, Kozytska I, Raks V, Badia R, Diaz-Garcia ME, Zaitsev VN (2014) Sensor Actuat B-Chem 200:198–205
11. Barja BC, Aramendia PF (2008) Photochem Photobiol Sci 7:1391–1399
12. Tan CL, Wang QM, Ma LJ (2010) Photochem Photobiol 86:1191–1196
13. Fu LS, Zhang HJ, Wang SB, Meng QG, Yang KY, Ni JZ (1999) J Sol–Gel Sci Technol 15:49–55
14. Sanchez C, Lebeau B, Chaput F, Boilot JP (2003) Adv Mater 15:1969–1994
15. Pinho SLC, Faneca H, Geraldes CFGC, Delville MH, Carlos LD, Rocha J (2012) Biomaterials 33:925–935
16. Liu FY, Fu LS, Wang J, Liu Z, Li HR, Zhang HJ (2002) Thin Solid Films 419:178–182
17. Zhao HJ, Bagwe RP, Tan WH (2004) Adv Mater 16:173–176
18. Gao CB, Lu ZD, Yin YD (2011) Langmuir 27:12201–12208
19. Zhou JM, Zhang WJ, Hong CY, Pan CY, Appl ACS (2015) Mater Inter 6:3618–3625
20. Polyakov B, Antsov M, Vlassov S, Dorogin LM, Vahtrus M, Zabels R, Lange S, Lohmus R (2014) Beilstein J Nanotechnol 5:1808–1814
21. Huang L, Ao LJ, Wang W, Hu DH, Sheng ZH, Su W (2015) Chem Commun 51:3923–3926
22. Goncalves MC, De V, Bermudez Z, Ferreira RAS, Carlos LD, Ostrovskii D, Rocha J (2004) Chem Mater 16:2530–2543
23. Ho JA, Chang HC, Su WT (2012) Anal Chem 84:3246–3253
24. Yoshimoto S, Sawaguchi T, Su W, Jiang JZ, Kobayashi N (2007) Angew Chem Int Ed 46:1071–1074
25. Elbanowski SLM, Makowska B, Hnatejko Z (2002) J Photochem Photobiol, A 150:233–247